Disorder effects and current percolation in FeAs-based superconductors

2010 Supercond. Sci. Technol. 23 054006

(http://iopscience.iop.org/0953-2048/23/5/054006)

Supercond. Sci. Technol. **23** (2010) 054006 (7pp) doi:10.1088/0953-2048/23/5/054006

Disorder effects and current percolation in FeAs-based superconductors

M Eisterer[1], M Zehetmayer[1], H W Weber[1], J Jiang[2], J D Weiss[2], A Yamamoto[2], E E Hellstrom[2], D C Larbalestier[2], N D Zhigadlo[3] and J Karpinski[3]

[1] Atominstitut, Vienna University of Technology, A-1020 Vienna, Austria
[2] National High Magnetic Field Laboratory, Florida State University, Tallahassee, FL 32310, USA
[3] Laboratory for Solid State Physics, ETH Zurich, CH-8093 Zurich, Switzerland

Received 1 December 2009, in final form 18 January 2010
Published 23 April 2010
Online at stacks.iop.org/SUST/23/054006

Abstract
We report the influence of atomic disorder introduced by sequential neutron irradiation on the basic superconducting properties, flux pinning and grain connectivity. Two different polycrystalline Sm-1111 samples ($SmFeAsO_{1-x}F_x$) and two Ba-122 single crystals ($BaFe_{1.8}Co_{0.2}As_2$) were investigated. The monotonic decrease of the transition temperature with neutron fluence degrades the upper critical field, at least in the investigated temperature region. Pinning, on the other hand, is largely improved, with a different optimal defect concentration (fluence) in the two materials. The analysis of the current flow in the polycrystalline samples reveals weak link behavior in the majority of grain connections and the existence of stronger grain connections. The density of the latter seems to be close to the percolation threshold (i.e. the minimum fraction for a continuous current path). Both types of connections are sensitive to disorder and degrade upon neutron irradiation.

(Some figures in this article are in colour only in the electronic version)

1. Introduction

The optimization of the superconducting properties, flux pinning and intergranular current flow are important issues for applications of superconductors, which can be addressed by neutron irradiation studies [1–9]. Fast neutrons introduce atomic disorder and, in many cases, pinning efficient defects. The enhanced impurity scattering potentially changes the transition temperature [3–9], the superconducting energy gap [4], the upper critical field [3, 5, 9] and the magnetic penetration depth [9]. These defects are a model system for naturally grown or artificially produced defects [5, 10] and help to understand sample-to-sample variations and to identify possible routes for material optimization [11]. Theoretical predictions can be checked [4] and limitations of the current flow identified [11, 12], since inter- and intragranular defects are differently affected. The influence of nanosized defects as bulk pinning centers was unambiguously demonstrated [1, 2, 7].

Fe-based superconductors offer promising superconducting properties, i.e. comparatively high transition temperatures [13–16] and high upper critical fields [17–19]. The intergranular current flow, however, seems to be problematic [20–25]. Very few irradiation studies on bulk samples [8, 26, 27] and single crystals [28] were performed until now.

In this paper we report the influence of neutron irradiation on the transition temperature, the upper critical field and flux pinning. The inter- and intragranular current flow is investigated.

2. Experimental details

One $SmFeAsO_{1-x}F_x$ sample (denoted as Sm-1111A in the following) was prepared at the National High Magnetic Field Laboratory. The starting materials of As, Sm, Fe, Fe_2O_3 and SmF_3 were mixed and pressed into a pellet, wrapped with Nb foil and sealed in a stainless steel tube. The sealed sample was heat-treated at 1160 °C for 6 h in a high temperature isostatic press under a pressure of 280 MPa. The main phase of the sample is $SmFeAsO_{1-x}F_x$, with a grain size of 10–15 μm. The impurity phases include SmAs, SmOF and FeAs. The size of the sample was $1.1 \times 1.7 \times 3.7$ mm^3.

The second polycrystalline sample of $SmFeAsO_{1-x}F_x$ (sample Sm-1111B) was synthesized at the ETH Zurich [29]. SmAs, FeAs, SmF_3, Fe_2O_3 and Fe were pulverized and sealed in a BN crucible. At a pressure of 3 GPa, the temperature was increased to 1350–1450 °C within 1 h. After keeping this temperature for 4.5 h, the crucible was quickly cooled down to room temperature. The sample investigated in this study was a piece of the pellet with an approximately triangular cross section (∼2.5 mm^2) and a height of 1.9 mm.

$BaFe_{1.8}Co_{0.2}As_2$ single crystals were prepared by the self-flux method [30] under a pressure of 280 MPa at the National High Magnetic Field Laboratory. One crystal was characterized resistively, another inductively. Typical dimensions of these crystals were $1.4 \times 0.7 \times 0.1$ mm^3.

Neutron irradiation was performed in the central irradiation facility of the TRIGA-Mark-II reactor in Vienna. The samples were sealed into a quartz tube and sequentially irradiated, starting with a fast neutron fluence ($E > 0.1$ MeV) of 4×10^{21} m^{-2}. The highest cumulative fluence was 1.8×10^{22} m^{-2}.

Neutrons transfer their energy to the lattice atoms by direct collisions. The transferred energy must exceed the binding energy of the lattice atom to displace it; thus only fast neutrons lead to defects. The size of defects is expected to range from point defects to several nanometers, as observed in the cuprates [31]. Self-shielding effects can be neglected, since the penetration depth of fast neutrons is of the order of a few centimeters, which is much larger than the sample dimensions. Only neutrons of low or intermediate energies are shielded efficiently because of large neutron cross sections at these energies. Some of these neutron capture reactions are followed by γ- or β-emission, which may produce single displaced atoms [28]. These reactions are restricted to the surface in Sm-1111, since Sm is a particular strong neutron absorber. The bulk will be penetrated only by fast neutrons. In contrast, the recoil from γ- and β-emission might also contribute to the total defect density in the bulk of Ba-122. However, since we do not find any significant difference in the change of the transition temperature in the two compounds after irradiation, defects seem to result predominantly from fast neutrons.

The resistivities of the sample Sm-1111A and of one Ba-122 crystal were measured at various fixed fields while cooling at a rate of 10 K h^{-1} with an applied current of 10 mA (single crystal: 300 μA). Current and voltage contacts were made by silver paste (single crystal: silver epoxy). The distance between the two voltage contacts was around 1 mm for the polycrystalline samples and around 0.3 mm for the crystal. The transition temperature and the upper critical field were determined by means of a 90% criterion.

Magnetization loops at various temperatures were recorded in a commercial 7 T SQUID magnetometer (sample Sm-1111A) and a commercial vibrating sample magnetometer (Ba-122). The critical current density was calculated from the magnetization loops using the Bean model. A self-field correction was made for the single crystal. The self-field was calculated numerically, averaged over the sample volume and added to the applied field $\mu_0 H$, leading to $J_c(B)$ [32]. J_c of sample Sm-1111A represents a rough estimation because of the uncertainty in the geometry of the current loops (grain size). The self-field correction was therefore abandoned ($J_c(\mu_0 H)$).

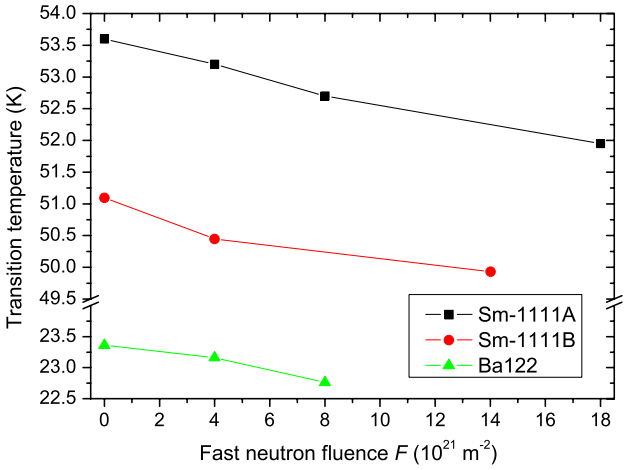

Figure 1. The transition temperatures of three samples as a function of the fast neutron fluence, F. The introduced disorder reduces T_c of all samples with a similar slope dT_c/dF.

The ac susceptibility at 33 Hz was measured in the same SQUID with an amplitude of 30 μT (Ba-122 single crystal: 100 μT) to determine T_c and the shielding fraction. The demagnetization factor, which is needed for estimating the shielding fraction, was calculated numerically for the actual sample geometry.

In addition, the remnant magnetic moment was measured (SQUID) as a function of the maximally applied field, H_{max}, in order to check for magnetic granularity [20, 24, 33, 34].

3. Results and discussion

Neutron irradiation introduces scattering centers, which increase the normal state resistivity. The normalized resistivity $\rho_{norm} := \rho(55\text{ K})/(\rho(300\text{ K}) - \rho(55\text{ K}))$ increased from 0.49 in the unirradiated sample Sm-1111A to 0.55, 0.61 and 0.72 after irradiation to a fluence, F, of 4, 8 and 18×10^{21} m^{-2}, respectively. The normalization to the phonon contribution ($\rho(300\text{ K}) - \rho(55\text{ K}) = 450 \pm 150$ $\mu\Omega$ cm) potentially cancels a reduction of the effective current-carrying cross section due to secondary phases, voids or cracks [35] and errors in the determination of the distance between the voltage taps. The nearly linear increase of ρ_{norm} with neutron fluence (∼1.3×10^{-23} m^2) indicates that the defect density scales with neutron fluence and that the resistivity is still far from saturation, where the mean free path of the charge carriers approaches the lattice parameter. The increase of impurity scattering is also shown by the resistivity ratio $\rho(300\text{ K})/\rho(55\text{ K})$, which decreases from 3.03 to 2.83, 2.64 and 2.38.

This resistivity ratio was only 2.2 in the Ba-122 single crystal and decreased to 1.9 after irradiation to 4×10^{21} m^{-2}. A clear increase of resistivity after irradiation is thus observed in both compounds, in single and polycrystals.

Neutron irradiation also decreases the transition temperature (figure 1) with a similar slope in both materials: $dT_c/dF = -9.1$, -7.75 and -7.5×10^{-23} K m^2 in Sm-1111A (resistive), Sm-1111B (inductive) and Ba-122 (inductive),

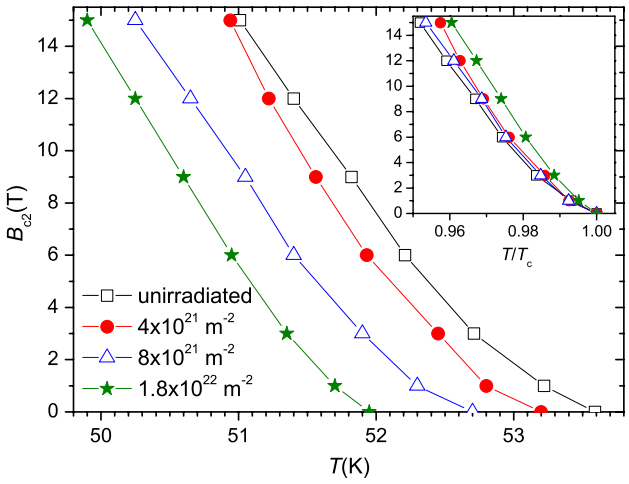

Figure 2. Temperature dependence of the upper critical field, B_{c2}, in sample Sm-1111A. The inset contain the same data, but the temperature was normalized by the transition temperature, T_c. The influence of neutron irradiation is dominated by the decrease in transition temperature. Nevertheless, the slope increases after neutron irradiation, having its maximum after the first irradiation step (4×10^{21} m^{-2}).

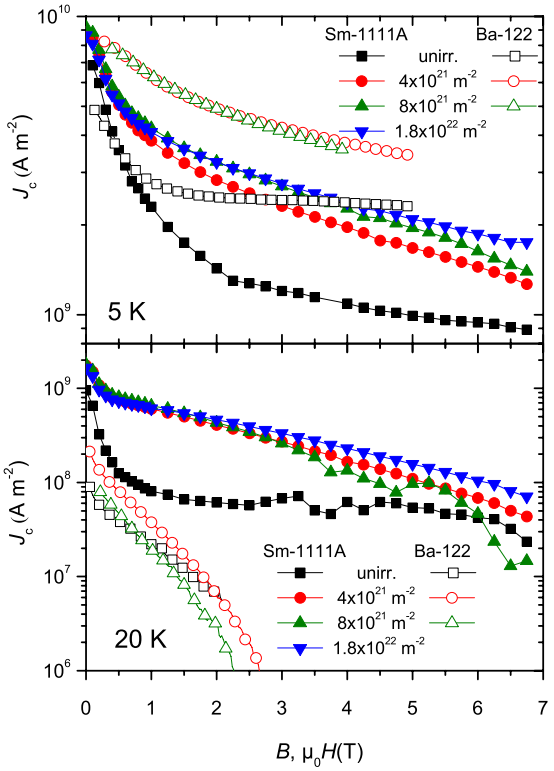

Figure 3. The critical current density increases in Sm-1111 (sample A, solid symbols) and Ba-122 (open symbols) due to the introduction of pinning-efficient defects by neutron irradiation. The x axis refer to B for the Ba-122 crystal and to $\mu_0 H$ for the Sm-1111 sample, since no self-field correction was made in the latter case. J_c is an estimate for the intragranular currents in Sm-1111.

respectively. This decrease of the transition temperature caused by impurity scattering is a general property of superconductors with anisotropic energy gap [36], and particularly with $s_{\pm}$ (extended s-wave [37]) gap symmetry [38], or a consequence of multiband superconductivity [4].

Karkin *et al* [26] found a complete suppression of superconductivity in La-1111 after irradiation to a fast neutron fluence of 1.6×10^{23} m^{-2}, which is about one order of magnitude higher than the highest fluence of the present study. The slope dT_c/dF found in our samples would predict a decrease in T_c of between 12 and 15 K at their neutron fluence. Either the decrease of T_c with neutron fluence does not stay linear at high fluences or their sample behaves differently. Note that T_c of the La-1111 sample was significantly more below optimum than that of our Sm-1111 samples.

The upper critical field of sample Sm-1111A near the transition temperature is presented in figure 2. The decrease in transition temperature shifts the $B_{c2}(T)$ curves to lower temperatures, but the slope increases after irradiation (see the inset). The interplay between the decrease in transition temperature and the increase in slope suggests the presence of a maximum in $B_{c2}(0)$ at around 4×10^{21} m^{-2}.

In the Ba-122 system, the slope of $B_{c2}(T)$ hardly changes after irradiation for $H \parallel ab$, leading to a general decrease of the upper critical field in this field orientation. $B_{c2}(T)$ becomes steeper for $H \parallel c$, which results in a reduction of the upper critical field anisotropy (e.g. from 2.8 to 2.5 at 22 K) [28]. Good agreement of the angular dependence of B_{c2} with anisotropic Ginzburg–Landau theory is found near T_c before and after irradiation.

3.1. Flux pinning

The critical current densities of the polycrystalline sample Sm-1111A and the single-crystal Ba-122 are compared before and after neutron irradiation to various fluences in figure 3. The single-crystal data refer to a well-defined crystallographic orientation of the applied field ($H \parallel c$) and the induced currents (parallel to the ab planes), whereas the magnetic moment of the polycrystalline sample results from currents flowing in all crystallographic directions providing only a rough estimate of the intragranular currents (see below). However, the magnitude and field dependence of J_c in both samples is similar at 5 K (upper panel), in particular after irradiation. Both materials show traces of a second peak (e.g. Ba-122 at 5 K and Sm-1111 at 20 K), which disappear after irradiation [8, 28]. The second peak effect is generally assumed to indicate the transition from a low J_c ordered vortex phase at low magnetic fields to a high J_c disordered phase at higher fields. Introducing more disorder shifts the transition field to lower values and eventually leads to the disappearance of the ordered phase, as is observed in our samples upon irradiation. The introduced defects are efficient pinning centers in both materials.

The self-field J_c increases after the first irradiation step, but does not change much upon further irradiation. Higher fluences decrease the field dependence of J_c in Sm-1111, but not in the Ba-122 single crystal, where the second irradiation step reduces J_c at 20 K, a consequence of the reduced transition temperature.

The temperature dependence of the critical current densities at 1 T is shown in figure 4. The relative enhancement

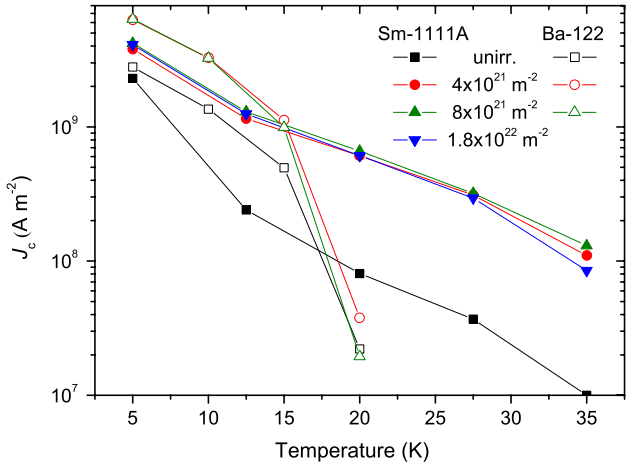

Figure 4. Critical current densities at 1 T in samples Ba-122 and Sm-1111A as a function of temperature prior to and after neutron irradiation to various fluences.

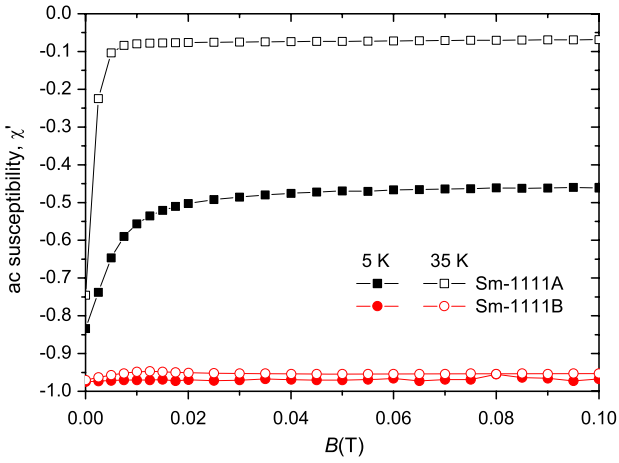

Figure 5. AC susceptibility as a function of the applied dc field. While the global currents are rapidly suppressed in sample Sm-1111A, they remain significant ($\gg 2.5 \times 10^4$ A m^{-2}) in sample Sm-1111B.

after irradiation (by up to one order of magnitude) increases with temperature (sample Sm-1111A, solid symbols), which indicates that the pinning energy of the radiation-induced defects can better compete with the thermal energy than the pinning energy of the as-grown defect structure. A reasonable explanation is a larger defect size, since J_c is not very sensitive to the defect density (fluence).

In the Ba-122 crystal, on the other hand, the temperature dependence hardly changes after irradiation: only at high temperatures the slope becomes slightly steeper, which is caused by the reduced transition temperature (20 K is close to T_c). The pinning energies of the as-grown and the radiation-induced defects seem to be similar.

3.2. Intra- and intergranular currents

The global current flow was checked by ac susceptibility measurements (figure 5). The ac susceptibility, χ', of sample Sm-1111A rapidly increases (shielding decreases) with applied dc field, which indicates a rapid decoupling of the grains. A metallic Fe–As wetting phase, which can be passed by the supercurrents only via Josephson tunneling, was found at the grain boundaries of a comparable sample [22]. These superconducting tunnel currents are known to be rapidly suppressed by magnetic fields.

Shielding is perfect ($\chi' = -1$) within experimental accuracy in sample Sm-1111B. This means that the supercurrents only flow at the sample surface and the penetration depth of the applied ac field ($\delta = H^{ac}/J_c$) is negligible compared to the smallest sample dimension R^s; thus, the intergranular currents must be *much larger* than $H^{ac}/R^s \approx 2.5 \times 10^4$ A m^{-2}. The field-independent susceptibility proves the existence of significant global currents, at least in the field region relevant for the measurement of the remnant magnetic moment. This does not necessarily mean that weak (Josephson) grain coupling is absent in this sample. However, the number of stronger grain connections must be significantly above the percolation threshold [39], which is defined as the minimum fraction for a continuous current path.

In order to investigate the influence of disorder on the inter- and intragranular currents, the remnant magnetic moment, m_{rem}, was measured as a function of the maximally applied field, H_{max} (e.g. solid circles in figure 6(b)). The magnetic moment was measured at each field H_{max} (figure 6(a)) and after reducing the field to zero (circles in figure 6(b)). If all current loops, which were induced by the application and removal of the external magnetic field, are of similar geometry, a peak in the derivative of the remnant magnetic moment with respect to the logarithm of the maximally applied magnetic field:

$$\frac{\mathrm{d}m_{rem}}{\mathrm{d}\log(H_{max})}, \qquad (1)$$

occurs, when H_{max} approximately equals the Bean penetration field $H^\star$ [40]. The critical current density can be estimated from $H^\star \approx J_c R$ if the representative geometry of the current loops, R, is known (typically the smallest sample or grain dimension).

Two peaks are observed in granular materials [40], if $J_c^{intra} R^g \ll J_c^{inter} R^s$, where J_c^{intra} and J_c^{inter} denote the critical current density within or between the grains, respectively, and R^s (R^g) is the smallest sample (grain) geometry. Flux first penetrates the whole sample along the grain boundaries, while the inner parts of the grains are still free of vortices. If the above condition is not fulfilled, the peaks overlap and cannot be properly distinguished.

The logarithmic derivative (1) of sample Sm-1111B is presented in figure 7. Two peaks occur at 20 and 35 K (also at 12.5 and 27.5 K, not shown) in the unirradiated state (solid squares). The low field peak is usually ascribed to intergranular currents shielding the whole sample. This peak is located at about 14 mT at 5 K (solid squares in figure 7(a)), which corresponds to a critical current density of around 10^7 A m^{-2}, decreasing to about 5×10^6 A m^{-2} at 35 K.

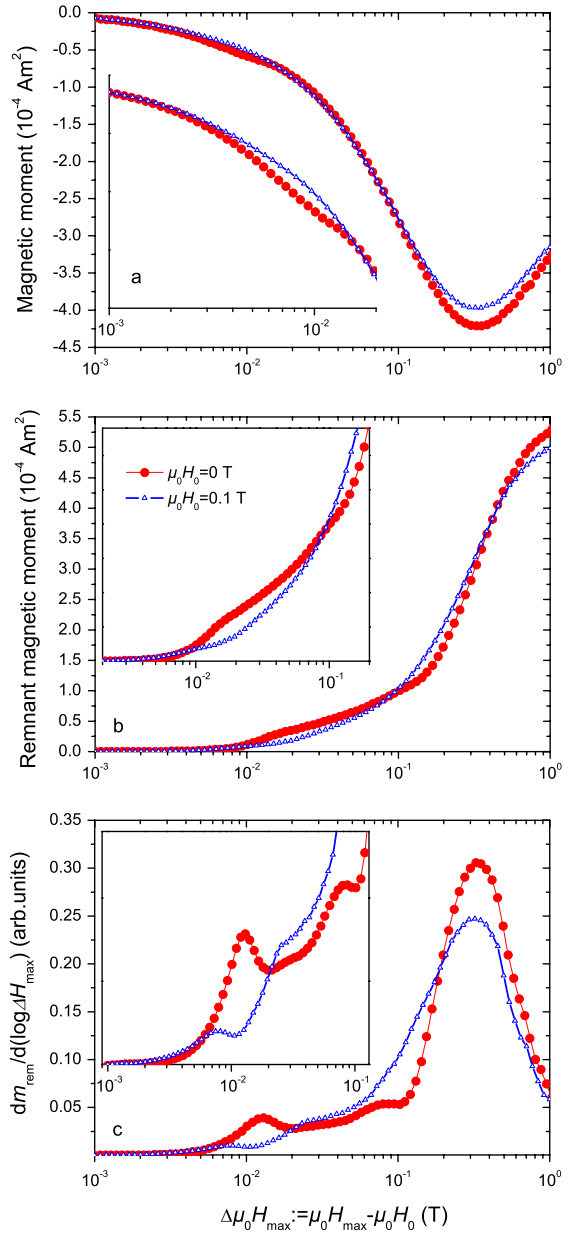

Figure 6. Magnetic moment as a function of the (increasing) applied magnetic field $\Delta\mu_0 H_{\rm max}$ (panel (a)). Measurements were done in a background field, $\mu_0 H_0$, of 0 T (circles) and 0.1 T (triangles). The field was reduced to $\mu_0 H_0$ between each value of $\mu_0 H_{\rm max}$ in order to measure the remnant magnetic moment $m_{\rm rem}$ (panel (b)). A peak occurs in d$m_{\rm rem}$/d(log $\Delta H_{\rm max}$) each time $\Delta H_{\rm max}$ approximately equals a penetration field (panel (c)). The low and high field peaks result from flux penetration into the whole sample (intergranular peak) and the grains (intragranular peak), respectively. All peaks shift to lower fields at $\mu_0 H_0 = 0.1$ T. The shift of the intergranular peaks is more pronounced, indicating a stronger field dependence of $J_{\rm c}^{\rm inter}$. Data were obtained at 5 K on sample Sm-1111B after the first irradiation step (4×10^{21} m^{-2}). The insets enlarge interesting details.

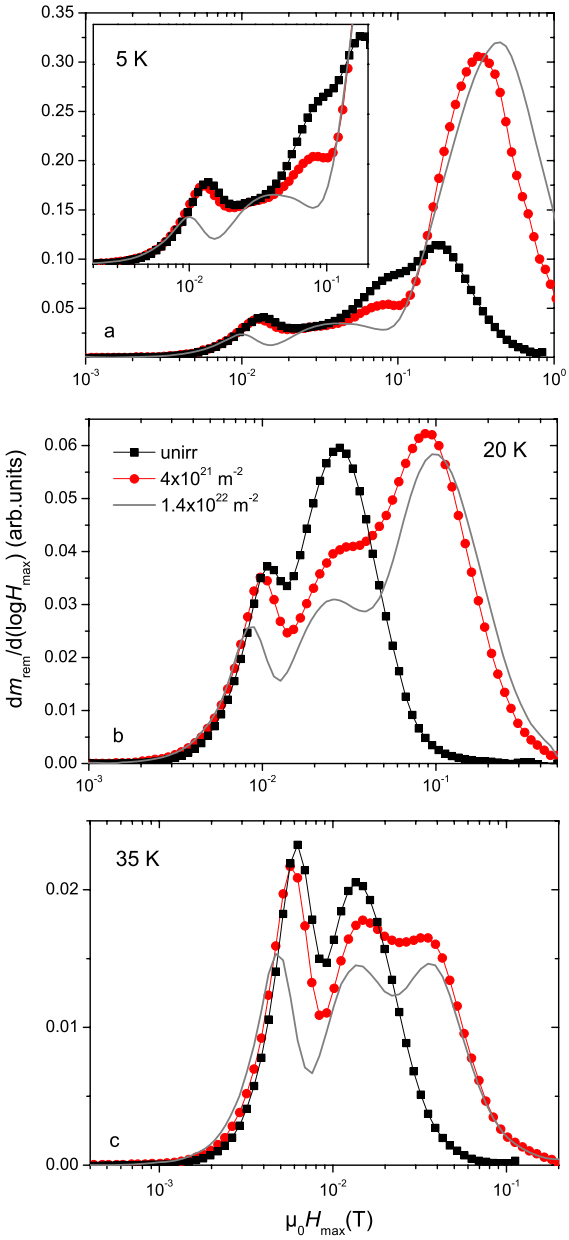

Figure 7. Evolution of the peaks in d$m_{\rm rem}$/d(log $H_{\rm max}$) (cf caption in figure 6, here with $\mu_0 H_0 = 0$ T) with temperature and neutron fluence. The irradiation reduces the intergranular currents (low and intermediate field peak). The intragranular (high field) peak shifts to higher fields, as a consequence of the increase in $J_{\rm c}^{\rm intra}$. The intermediate and high field peaks merge at temperatures above about 10 K in the unirradiated sample (Sm-1111B).

It is *a priori* not clear whether the low field peak simply arises from a rapid flux penetration immediately after $H_{\rm max}$ exceeds the lower critical field, $H_{\rm c1}$, of the sample, since the reversible magnetization strongly changes around $H_{\rm c1}$. In order to exclude this scenario, the measurement was repeated after field cooling the sample at 0.1 T. The measurement sequence was repeated with this constant offset field, $\mu_0 H_0 = 0.1$ T. The field was increased by $\Delta H_{\rm max}$ and decreased to 0.1 T, where the trapped magnetic moment was measured. The results at 5 K are compared to the standard measurements ($\mu_0 H_0 = 0$ T) in figure 6 (the moment measured immediately after field cooling was subtracted). The low field peak persists, but shifts to lower fields (by a factor of 1.7), which is a result of the field dependence of the critical currents. As can be seen in the inset of panel (b), the remnant magnetic moment is larger (between $\Delta\mu_0 H_{\rm max} = 2$ and 8 mT) first at 0.1 T, which results from an

earlier flux penetration (cf panel (a)). Then the larger critical currents at 0 T lead to a larger trapped flux, until the same behavior is repeated near the high field peak (m_{rem} at 0.1 T first larger then smaller than in zero field). In any case, the low field peak is well above the first penetration field and is obviously not caused by the reversible magnetization, which confirms its interpretation as an intergranular peak.

Neutron irradiation shifts the intergranular peak to lower fields (figure 7), which indicates a degradation of the intergranular currents. The effect is small after irradiation to 4×10^{21} m^{-2} (circles), but significant at 1.4×10^{22} m^{-2} (line graph). Such a degradation of the intergranular currents after neutron irradiation was also found in Bi tapes [12, 41] and coated conductors [42].

The high field peak usually originates from the intragranular currents shielding only individual grains [20, 34, 40]. In sample Sm-1111B, however, the high field peak splits at 5 K, which sheds some doubts on this standard interpretation. A similar peak split at 5 K was reported for a polycrystalline Nd-1111 sample [20]. Three peaks are clearly visible at all temperatures after neutron irradiation (solid line in figure 7).

It will be argued in the following that the intermediate field peak is caused by clusters of better connected grains and that the high field peak is the intragranular peak. These two peaks are only visible at 5 K in the unirradiated sample and merge at 12.5, 20, 27.5 and 35 K. This temperature dependence excludes the scenario where the two peaks are caused by currents of the same magnitude flowing on different length scales (e.g. grains and clusters, or grains (clusters) of different sizes). This is confirmed by the changes after irradiation, which are quite different for these peaks. While the high field peak shifts to higher fields, the intermediate peak shows a less systematic behavior. It shifts to lower fields at 5 and 12.5 K but approximately retains its position at higher temperatures (figure 7). The shift of the high field peak obviously results from improved pinning (larger intragranular currents, see section 3.1) which also enhances the hysteresis (e.g. larger saturated remnant moment). The decrease of the intermediate peak field at low temperatures after irradiation indicates that the corresponding currents are limited by grain boundaries. This scenario is supported by the field dependence of the peak positions (figure 6). While the high field peak shifts only by about 5%, the low and intermediate peak fields decrease by a factor of roughly two due to the increase of the background field from 0 (solid circles) to 0.1 T (open triangles). (The intermediate field peak degrades to a bump at 0.1 T.)

Only a rough estimate can be given for J_c in the current loops which are responsible for the intermediate peak. Since the size of the loops must be smaller than the sample geometry and larger than the individual grains, the corresponding current density is between 2×10^8 and 2×10^9 A m^{-2} at 5 K and 0 T.

At least two types of grain connections exist in our polycrystalline samples: (i) the wetted grain boundaries (type A), whose currents are rapidly suppressed by magnetic fields and (ii) grain boundaries over which currents can also pass at high magnetic fields (type B). The number of type-B connections is below the percolation threshold in sample Sm-1111A and above the percolation threshold in sample Sm-1111B, as indicated by the ac susceptibility. The rapid decrease of χ' directly shows the suppression of global currents after 'switching-off' type-A connections by applying an external magnetic field. It was pointed out in [22] that samples of apparently similar microstructures (probed by x-ray and SEM) showed a large variation in the intergrain current density. It is therefore reasonable to assume that the number of type-B connections is close to, but below, the percolation threshold in our sample Sm-1111A. In fact, the low field peak was not present in this sample, since the global currents were too small, but we observed the intermediate and high field peaks (at comparable fields) which might just reflect the structure of the incipient spanning cluster at the percolation threshold. In the 'nodes, links and blobs' picture, the incipient spanning cluster is composed of blobs which are connected by links [43]. Removing one link decomposes the spanning cluster, while blobs are multiply connected sites (clusters of type-B connected grains). The two peaks in sample Sm-1111A could correspond to flux penetration into the blobs and grains, respectively. In a comparable sample which obviously contained a spanning cluster of type-B connections, the links were made directly visible by scanning laser microscopy [22].

In sample Sm-1111B, the density of type-B connections seems to be significantly above the percolation threshold, since shielding of very small ac fields was nearly perfect (see above). However, the clusters of type-B connected grains may persist well above the percolation threshold and be responsible for the intermediate field peak.

4. Conclusions

Atomic scale disorder is not a promising way of improving the basic superconducting properties (B_{c2}, T_c) in Fe-based superconductors. Bulk pinning, on the other hand, is strengthened by the introduction of nanoscale defects. The critical current densities in the grains generally increase after the first irradiation step (fast neutron fluence: 4×10^{21} m^{-2}), but start to decrease again upon further irradiation in the Ba-122 single crystal, while a further improvement is found at high fields in Sm-1111 up to a fluence of 1.8×10^{22} m^{-2}.

We found indications that the majority of grain connections are weak links which decouple in magnetic fields. We identify a second type of connection over which supercurrents flow at high fields in a percolative manner, since their density seems to be close to the percolation threshold.

Acknowledgments

Work at ETH Zurich was supported by the Swiss National Science Foundation through the NCCR program MaNEP. Work at NHMFL was supported under NSF Cooperative Agreement DMR-0084173, by the State of Florida, and by AFOSR under grant FA9550-06-1-0474. Supported by the Austrian Science Fund under contract 21194.

References

[1] Meier-Hirmer R, Küpfer H and Scheurer H 1985 *Phys. Rev.* B **31** 183
[2] Zehetmayer M, Eisterer M, Jun J, Kazakov S M, Karpinski J, Birajdar B, Eibl O and Weber H W 2004 *Phys. Rev.* B **69** 054510
[3] Putti M *et al* 2005 *Appl. Phys. Lett.* **86** 112503
[4] Putti M, Affronte M, Ferdeghini C, Manfrinetti P, Tarantini C and Lehmann E 2006 *Phys. Rev. Lett.* **96** 077003
[5] Krutzler C, Zehetmayer M, Eisterer M, Weber H W, Zhigadlo N D and Karpinski J 2007 *Phys. Rev.* B **75** 224510
[6] Wilke R H T, Bud'ko S L, Canfield P C, Farmer J and Hannahs S T 2006 *Phys. Rev.* B **73** 134512
[7] Sauerzopf F M 1998 *Phys. Rev.* B **57** 10959
[8] Eisterer M, Weber H W, Jiang J, Weiss J D, Yamamoto A, Polyanskii A A, Hellstrom E E and Larbalestier D C 2009 *Supercond. Sci. Technol.* **22** 065015
[9] Ossandon J G, Thompson J R, Kim Y C, Sun Y R, Christen D K and Chakoumakos B C 1995 *Phys. Rev.* B **51** 8551
[10] Eisterer M, Müller R, Schöppl R, Weber H W, Soltanian S and Dou S X 2007 *Supercond. Sci. Technol.* **20** 117
[11] Eisterer M, Krutzler C and Weber H W 2005 *J. Appl. Phys.* **98** 033906
[12] Tönies S, Weber H W, Guo Y C, Dou S X, Sawh R and Weinstein R 2001 *Appl. Phys. Lett.* **78** 3851
[13] Ren Z-A *et al* 2008 *Chin. Phys. Lett.* **25** 2215
[14] Ren Z-A *et al* 2008 *Europhys. Lett.* **83** 17002
[15] Yang J *et al* 2008 *Supercond. Sci. Technol.* **21** 082001
[16] Rotter M, Tegel M and Johrendt D 2008 *Phys. Rev. Lett.* **101** 107006
[17] Jaroszynski J *et al* 2008 *Phys. Rev.* B **78** 064511
[18] Senatore C, Flükiger R, Cantoni M, Gu W, Liu R H and Chen X H 2008 *Phys. Rev.* B **78** 054514
[19] Yamamoto A *et al* 2009 *Appl. Phys. Lett.* **94** 062511
[20] Yamamoto A *et al* 2008 *Supercond. Sci. Technol.* **21** 095008
[21] Kametani F *et al* 2009 *Supercond. Sci. Technol.* **22** 015010
[22] Kametani F *et al* 2009 *Appl. Phys. Lett.* **95** 142502
[23] Lee S *et al* 2009 *Appl. Phys. Lett.* **95** 212505
[24] Otabe E S *et al* 2009 *Physica* C **469** 1940
[25] Tamegai T, Nakajima Y, Tsuchiya Y, Iyo A, Miyazawa K, Shirage P M, Kito H and Eisaki H 2009 *Physica* C **469** 915
[26] Karkin A E, Werner J, Behr G and Goshchitskii B N 2009 *Phys. Rev.* B **80** 174512
[27] Moore J D *et al* 2009 *Supercond. Sci. Technol.* **22** 125023
[28] Eisterer M, Zehetmayer M, Weber H W, Jiang J, Weiss J D, Yamamoto A and Hellstrom E E 2009 *Supercond. Sci. Technol.* **22** 095011
[29] Zhigadlo N D, Katrych S, Bukowski Z, Weyeneth S, Puzniak R and Karpinski J 2008 *J. Phys.: Condens. Matter* **20** 342202
[30] Sefat A S, Jin R, McGuire M A, Sales B C, Singh D J and Mandrus D 2008 *Phys. Rev. Lett.* **101** 117004
[31] Frischherz M C, Kirk M A, Zhang J P and Weber H W 1993 *Phil. Mag.* A **67** 1347
[32] Wiesinger H P, Sauerzopf F M and Weber H W 1992 *Physica* C **203** 121
[33] Müller K-H, Andrikidis C, Liu H K and Dou S X 1994 *Phys. Rev.* B **50** 10218
[34] Tönies S, Vostner A and Weber H W 2002 *J. Appl. Phys.* **92** 2628
[35] Rowell J M 2003 *Supercond. Sci. Technol.* **16** R17
[36] Millis A J, Sachdev S and Varma C M 1988 *Phys. Rev.* B **37** 4975
[37] Mazin I I, Singh D J, Johannes M D and Du M H 2008 *Phys. Rev. Lett.* **101** 057003
[38] Bang Y, Choi H-Y and Won H 2009 *Phys. Rev.* B **79** 054529
[39] Eisterer M, Emhofer J, Sorta S, Zehetmayer M and Weber H W 2009 *Supercond. Sci. Technol.* **22** 034016
[40] Müller K-H, Andrikidis C, Du J, Leslie K E and Foley C P 1999 *Phys. Rev.* B **60** 659
[41] Hu Q Y, Weber H W, Sauerzopf F M, Schulz G W, Schalk R M, Neumüller H W and Dou S X 1994 *Appl. Phys. Lett.* **65** 3008
[42] Eisterer M, Fuger R, Chudy M, Hengstberger F and Weber H W 2010 *Supercond. Sci. Technol.* **23** 014009
[43] Coniglio A 1982 *J. Phys. A: Math. Gen.* **15** 3829